Nanoscale Advances

ROYAL SOCIETY OF CHEMISTRY

PAPER

View Article Online
View Journal | View Issue

Cite this: *Nanoscale Adv.*, 2025, **7**, 5625

A mechano-enzymatic method to produce nano/microcellulose with ancestral endoglucanase. A comparative study†

Ane Rivas-Zúñiga,[ab] Arantxa Eceiza *[b] and Borja Fernández-d'Arlas*[cd]

Received 28th May 2025
Accepted 17th July 2025

DOI: 10.1039/d5na00524h

rsc.li/nanoscale-advances

Given the abundance of cellulose and the potential of nano/microcellulose, here in this work we analyze the prospects of five cellulosic sources for obtaining nano/microcellulose. We assess the impact of three different enzymes (ancestral reconstructed endoglucanase, cellulase and α-amylase) on a mechano-enzymatic process. The characterization of the resulting material has been carried out using spectroscopic, diffraction, thermal and morphological techniques. The results indicate that enzymatic extraction slightly contributes to the increase in nano/microcellulose extraction efficiency, reaching ~12.5% with endoglucanase, which is higher than the ~8% achieved without the enzyme, increases the degree of crystallinity of the sample without altering the structure and chemical composition and hardly decreases the crystallite size. These findings contribute to understanding the role of enzyme technology in the development of novel sustainable cellulose based materials, when pursuing economic and environmental benefits.

1 Introduction

The past few decades have witnessed a significant surge in the exploration of polymeric and composite materials derived from renewable sources, reflecting both industrial and scientific interests.[1] Cellulose, as the most abundant and renewable biopolymer on Earth, stands out as a promising raw material due to its unique properties and versatile applications.[2,3]

The intrinsic properties of nanocellulose have motivated intense research pursuing innovative applications.[4] Nanocellulose, categorized into cellulose nanocrystals (CNCs), also known as nano-whiskers, cellulose nanofibrils (CNFs), and microfibrillated cellulose (MFC), preserves the biodegradability and biocompatibility of cellulose while offering enhanced properties such as high specific strength, large specific surface area, high aspect ratio and high crystallinity.[5–7] The properties of these materials promise practical applications in commercial products driven by their nature, properties, size, and functionalities. The high crystallinity of the material supports its use as a gas barrier, due to the difficulty that gas molecules face in passing through crystalline domains.[8] Crystallinity has a similar effect in preventing the penetration of certain particles, such as grease,[9] due to the tortuosity of the material. Its large specific surface area promotes the absorption and retention of gases, which is useful for packaging, as it allows for regulating oxygen or moisture inside.[10] Also, this high specific surface area allows materials like micro- or nano-celluloses to enhance the rigidity and strength of a product without increasing its weight. This could be a great advantage for the production of certain bio-nanocomposites.[9,11,12]

Various cellulose to nanocellulose conversion methods, including acid[4] and enzymatic hydrolysis,[13] ionic liquid treatment,[12] or combined treatments in which mechanical forces are also applied in addition to the above processes,[14] have been employed to obtain highly purified nanocellulose from different renewable sources such as cotton and wood,[15] or from wastes such as waste office paper[16] and waste tissue paper.[3] In nature, cellulases, a multicomponent enzyme system, play a crucial role in catalyzing the hydrolysis of cellulose, with endoglucanase and cellobiohydrolase being the primary enzymes involved.[2] In addition to the previous extraction advancements, it has been demonstrated that the combination of enzymatic hydrolysis with mechanical forces enhances the hydrolysis reaction yield, achieving an increase in the aspect ratio of the fibers.[14,17] Spagnuolo *et al.*[18] reported that incorporating a 10 minute ball milling step prior to the enzymatic treatment led to a 9% increase in extraction yield compared to enzymatic treatment alone. Remarkably, extending the milling duration to 50 minutes resulted in a yield improvement of up to 69%.

[a]CIC-NanoGUNE, Avenida de Tolosa 76, 20018, Donostia-San Sebastian, Spain
[b]'Materials+Technologies' Group, Chemical & Environmental Engineering Department, Faculty of Engineering of Gipuzkoa, University of the Basque Country (UPV/EHU), Plaza Europa 1, 20018, Donostia-San Sebastian, Spain. E-mail: arantxa.eceiza@ehu.eus
[c]Evolgene Genomics S.L, Avenida de Tolosa 76, 20018, Donostia-San Sebastian, Spain
[d]Siemens-Gamesa, Avenida Ciudad de la Innovación 2, 31621, Sarriguren, Spain

† Electronic supplementary information (ESI) available. See DOI: https://doi.org/10.1039/d5na00524h

Furthermore, the evolution of enzyme technology presents promising avenues for cellulose utilization and processing. Ancestral sequence resurrection has emerged as a novel approach to engineering enzymes, offering enhanced thermal operability and activity under demanding industrial conditions.[19] Reconstructing ancestral endoglucanases from ancient bacterial species, researchers have demonstrated superior enzyme efficiency over a wide range of temperatures and pH levels, alongside enhanced substrate usage and catalytic promiscuity.[13] These findings hold significant implications for industrial bioprocessing, particularly in the context of sustainable bioproduct generation from cellulose-rich substrates. This was demonstrated by Alonso-Lerma *et al.*,[20] who reported extraction yields of approximately 15% after 24 hours of incubation at 50 °C using the ancestral endoglucanase, substantially higher than the 3–5% obtained with other commercial endoglucanases.

In conclusion, the integration of enzymatic processes into nanocellulose production and the exploration of cellulose at the nanoscale, oriented towards recycling initiatives, emphasize a multifaceted approach to sustainable biomaterial development. Leveraging these advancements offers promising avenues for addressing environmental challenges and fostering the transition toward a circular economy.

In this work, the enzymatic activity towards nano/microcellulose (NMC) generation of a reconstructed endoglucanase (EmNMC) was compared with a commercial cellulase and with an α-amylase. To identify the most suitable cellulose source for NMC production, a preliminary screening was conducted using various substrates, including Avicel, production paper, filter paper, cleaning paper, and Kraft pulp, without using any additional pretreatment step. Based on extraction yields, filter paper was selected as the optimal substrate. Subsequently, an exhaustive study of the properties of the NMCs produced from filter paper was carried out using various physico-chemical, thermal and morphological characterization techniques such as Fourier-Transform Infrared Spectroscopy (FTIR), X-ray Diffraction (XRD), Thermogravimetric Analysis (TGA), Dynamic Light Scattering (DLS), Atomic Force Microscopy (AFM), and Scanning Electron Microscopy (SEM). This study focuses on a detailed characterization to understand the effect of the incubation time on the morphology or chemical composition of the resulting material.

2 Materials and methods

2.1 Raw materials

Commercial filter paper (Whatman Lot. 17723451), containing only cellulose, was used as the substrate for NMC production. In order to analyze the yield of the process, it was compared with four other substrates as cellulose sources: cleaning paper (Vadrisa, 1200), Avicel PH-101 (Sigma-Aldrich Lot. BCBW4188), Kraft pulp (Zicuñaga paper mill, Hernani, Spain) and Lapponian paper (Dr Kurt Müller). A summary was prepared, providing the cellulose percentage and the production method for each substrate based on the available information obtained from each supplier (Table S1†). As part of the study, in addition to the reconstructed ancestral endoglucanase, some other commercial hydrolytic enzymes were used to compare the extraction yields: α-amylase (Sigma-Aldrich, 10065) from *Aspergillus oryzae* and cellulase (Sigma-Aldrich, 22178) from *Aspergillus niger*, both produced by fungi.

2.2 Ancestral endoglucanase reconstruction

The ancestral endoglucanase sequence used to produce NMC was previously developed by the Nanobiotechnology group at CIC nanoGUNE.[13] To summarize the whole process of reconstructing the ancestral sequence, the following steps were undertaken.

First, *Bacillus subtilis* was chosen as the query sequence for the reconstruction due to its importance in the industrial sector, and a list of homologous sequences of organisms from different phyla (Firmicutes, Proteobacteria and Actinobacteria) was obtained from the US National Center of Biotechnology Information (NCBI).[21] Then, applying some bioinformatic tools such as Molecular Evolutionary Genetics Analysis (MEGA), MUltiple Sequence Comparison by Log-Expectation (MUSCLE) and Bayesian Evolutionary Analysis Sampling Trees (BEAST), among others, the alignment of the sequences was performed and cleaned manually to get the best reconstructed phylogenetic tree. Finally, Phylogenetic Analysis by Maximum Likelihood (PAML) software was used to carry out the reconstruction of ancestral sequences from the selected phylogenetic tree shown in Fig. 1A.

Three nodes were selected, corresponding to the reconstructed enzyme sequences, which were dated according to fossil estimates and divergences collected by Time tree of Life: Last Firmicutes Common Ancestor (LFCA), Last Clostridia Common Ancestor (LCCA) and Last Actinobacteria Common Ancestor (LACA).

2.3 Endoglucanase production and purification

Three ancestral endoglucanase DNA sequences obtained as described in Section 2.2. were sent to an external company (GenScript, New Jersey, USA). The company synthesized the endoglucanase sequences, linked them to a 6-histidine tag and cloned them into three different pQE80L vectors, forming three plasmids, as shown in the first steps represented in Fig. 1C. The codon usage was optimized for expression in *Escherichia coli*.

After that, *E. coli BL21* (Life Technologies, California, USA) was transformed with the plasmid, and the transformed cells were mixed with 1 L of Luria-Bertani (LB) medium and 1 mL of 0.1% w/v carbenicillin and grown in an incubator (Multitron Standard, Infors HT) at 37 °C and 4 × *g* for around 8 h until the optical density (OD_{600}) is 0.6–0.8. Then, the cell overproduction was induced using 1 mL of 0.1% w/v isopropyl β-D-1-thiogalactopyranoside (IPTG) and the culture was incubated at 37 °C and 4 × *g* overnight (around 16 h). After the induction period, the culture was centrifuged to separate the bacteria from the medium. The centrifugation conditions were 14 500 × *g*, at 4 °C for 20 minutes (Sorvall Lynx 4000, Thermo Scientific) and then the supernatant was discarded.

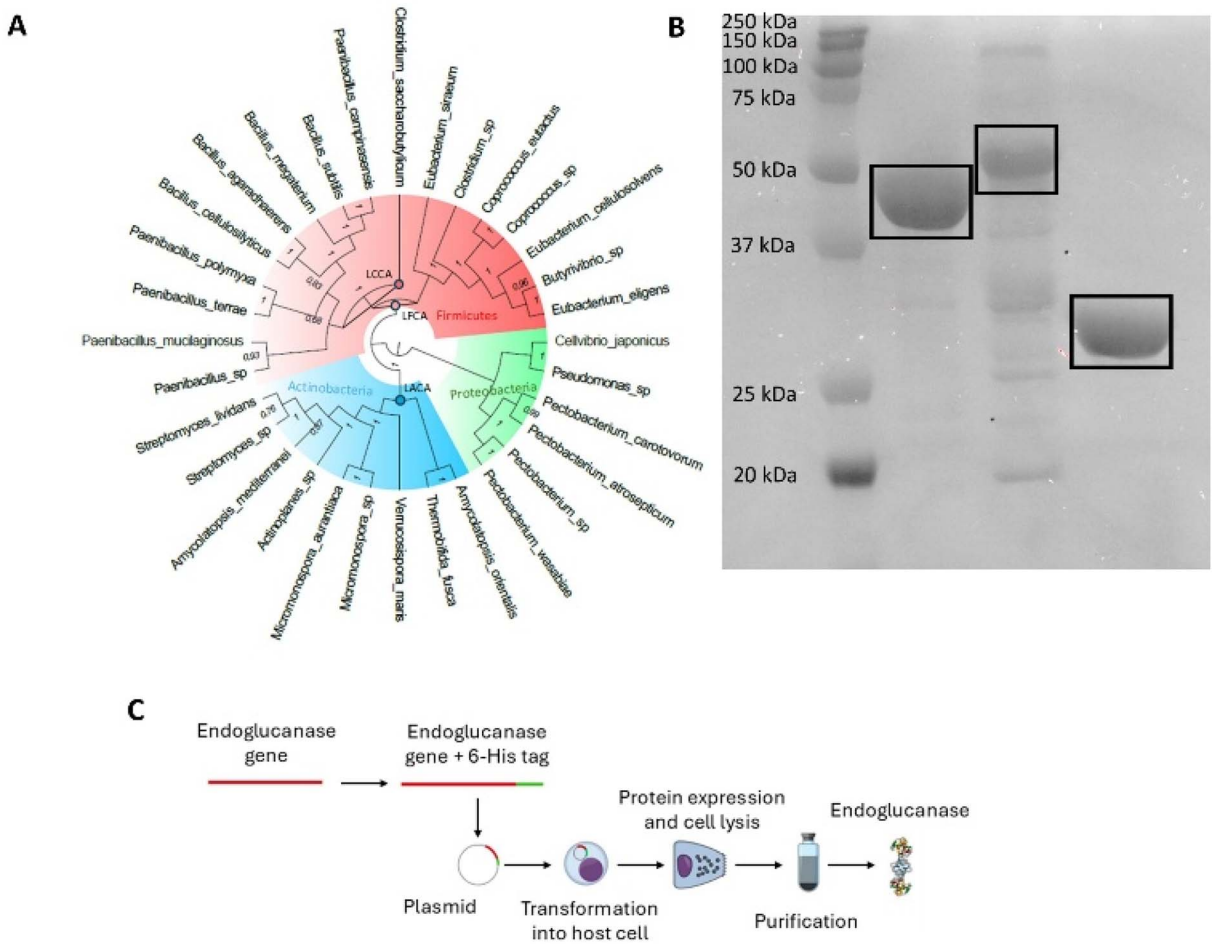

Fig. 1 (A) Phylogenetic tree of the ancestral endoglucanase adapted from Barruetabeña *et al.*;[13] (B) SDS-PAGE of α-amylase, cellulase and ancestral endoglucanase (from left to right). The concentration of the samples loaded onto the acrylamide gel was around 3.3 mg mL; 25 mg mL; 50 mg mL^{-1}, respectively; (C) scheme of the endoglucanase production and purification protocol.

With the aim of breaking the cell membrane, the pellet of 1 L of culture was resuspended in 15 mL of 50 mM sodium-phosphate buffer (pH 7) containing 300 mM NaCl. The cell disruption was done by sonication. The resuspended cells were sonicated in ice for 5 cycles of 30 seconds on and 4 minutes off using an amplitude of 70% (Vibra-cell 75115, Bioblock Scientific). Once the sonication was finished, the lysed cells were centrifuged at 33 000 × *g*, 4 °C for 50 minutes (Sorvall Lynx 4000, Thermo Scientific). Then, the supernatant containing proteins from 1 L of culture was collected and mixed with 5 mL of cobalt affinity resin (HisPur Cobalt Resin, Thermo Scientific), before being deposited in a polypropylene column (disposable 10 mL polypropylene columns, Thermo Scientific). Once the endoglucanase was bound to the Co^{2+} ions of the resin *via* the 6-histidine tag, the non-bounded proteins were eluted using 10 mL of 50 mM sodium-phosphate buffer (pH 7) containing 300 mM NaCl. Finally, in order to elute the endoglucanase, 10 mL of 50 mM sodium-phosphate buffer (pH 7, 300 mM NaCl) and 150 mM imidazole were added to detach the 6-histidine tag linked to the endoglucanase from the Co^{2+} ions of the resin. From each 1 L of cell culture, 0.5 g of endoglucanase were collected.

Once the protein was eluted, 12% v/v sodium dodecyl-sulfate polyacrylamide gel electrophoresis (SDS-PAGE) was run to verify that the purification was successfully completed. 15 μL of each sample were mixed with 15 μL of loading buffer, composed of Laemmli sample buffer and 2-mercaptoethanol, and heated for 5 minutes at 95 °C. 10 μL of protein ladder and each sample were charged onto the gel well, the gel was run (Mini Gel Tank, Invitrogen) for 1 h and then developed (Molecular Image Gel Doc XR+, Bio-Rad). The weight of the ancestral endoglucanase was ∼33 kDa and therefore the protein band should appear between the reference ladder bands of 15 and 35 kDa, as seen in Fig. 1B. The endoglucanase was stored in the elution buffer (50 mM sodium-phosphate buffer (pH 7, 300 mM NaCl) and 150 mM imidazole) in a refrigerator at 4 °C.

This protocol was performed in parallel with the three reconstructed endoglucanase sequences and, after performing some activity tests, the LFCA node was chosen as the best sequence because it was the enzyme that showed the greatest efficiency in a wider range of pHs at high temperatures.[13]

Also, in order to determine the size difference between the ancestral endoglucanase and the other commercial hydrolytic

enzymes used in the study (α-amylase and cellulase), an acrylamide gel was tested, as shown in Fig. 1B.

2.4 Nano/microcellulose production

The substrates were cut by hand and homogenized using a blender for 5 minutes at the maximum speed in order to facilitate the subsequent action of the enzyme on the different substrates. After producing the endoglucanase, 40 g of cellulose substrate were mixed with 1 L of deionized water, and 5 mg of enzyme per gram of substrate were added and incubated at 50 °C in a 230 rpm orbital stirrer for five different times: 1, 5, 24, 48 and 72 h, as shown in Fig. 2A. Although Barruetabeña *et al.*[13] showed slightly higher enzymatic activity at pH 5 compared to pH 7, pH 7 was chosen to align with more scalable and industrially relevant conditions, since maintaining acidic pH at larger scales can be challenging and may increase process complexity and cost. To quantify the impact of the enzyme on the extraction yield, a blank without enzymes for each incubation time was also performed.

After incubation, the mixture was tip sonicated (Vibracell 75115 sonicator, Bioblock Scientific) in an ice bath for 2 h, with 30 second on/off cycles, at 30% amplitude. Then, 8 L of deionized water were added in order to recover the NMC from the substrate. NMC isolation was performed by mixing the hydrolysate with deionized water, followed by centrifugation at 4200 × *g* for 5 minutes at 4 °C to remove larger particulates from the substrate. The resulting supernatant, containing the dispersed NMC (approximately 8 L), was then subjected to ultracentrifugation at 14 500 × *g* for 45 minutes at 4 °C to ensure the removal of any residual endoglucanase. The NMC was recovered as a pellet at the bottom of the centrifuge tube. Prior to testing the samples, part of the NMC was lyophilized (LyoQuest lyophilizer, Telstar) for 24 h *via* the freeze-drying method in order to perform some characterization tests, and the other part was kept in aqueous solution to carry out the morphological tests (AFM and SEM). A similar procedure was carried out with the commercial α-amylase and cellulase in order to assess the impact of different enzymes and the effect of a purely mechanical process (*i.e.*, the blank of the process).

The NMCs were designated EmNMC (Em for enzyme + mechanical stimulus) and mNMC (m for only mechanical stimulus), respectively, depending on whether or not enzymes

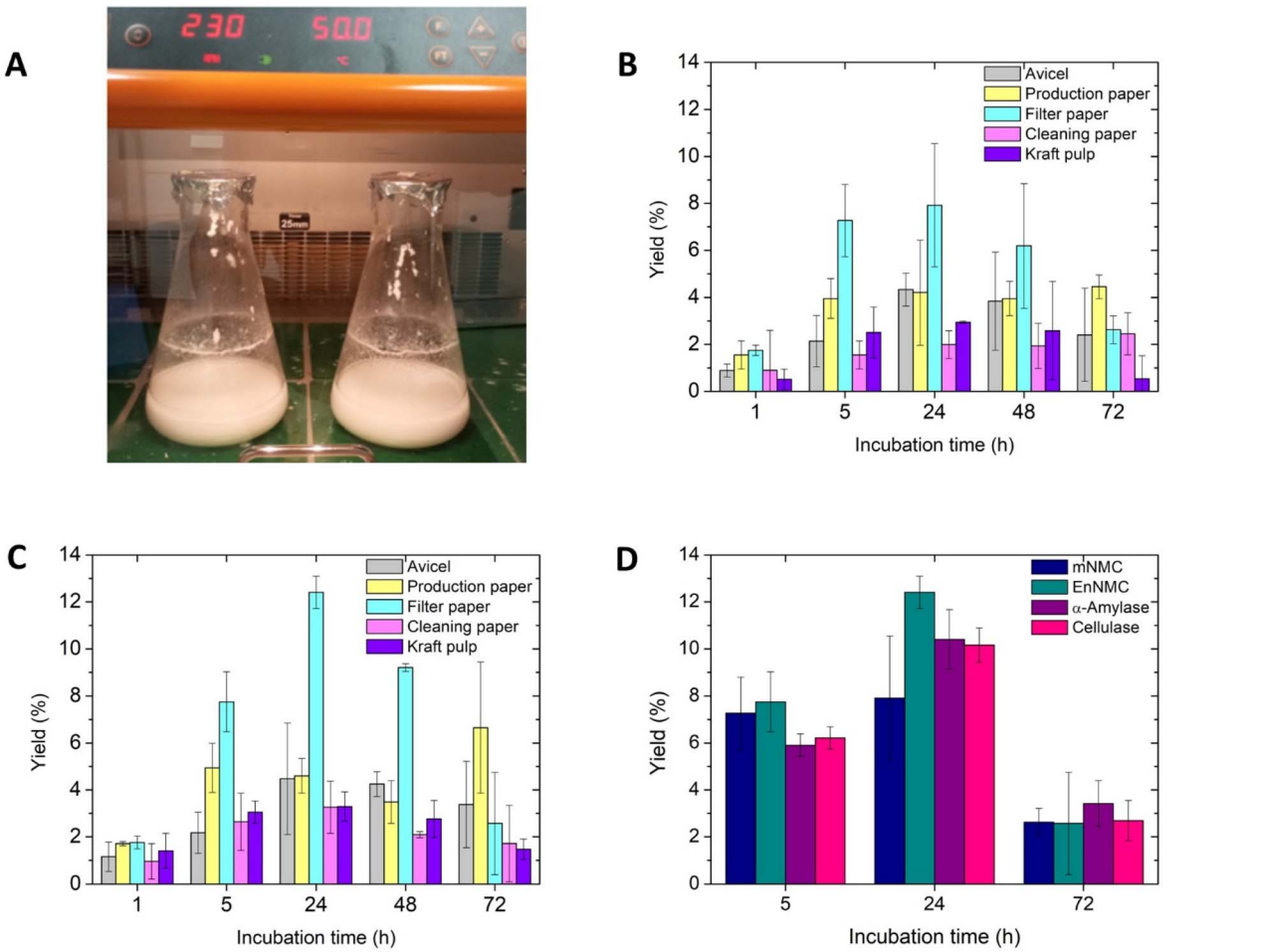

Fig. 2 (A) Flask incubation for NMC extraction; (B) extraction yields of mNMC using five different substrates and different incubation times. Error bars indicate standard error (SE; $n = 3$); (C) extraction yields of EmNMC using five different substrates and different incubation times. Error bars indicate standard error (SE; $n = 3$); (D) extraction yields using three hydrolytic enzymes (EmNMC, $EmNMC_{\alpha\text{-amylase}}$, and $EmNMC_{cellulase}$) using filter paper as the substrate at different incubation times. Error bars indicate standard error (SE; $n = 3$).

were used to produce them. NMCs produced using α-amylase or cellulase were specified as $EmNMC_{\alpha\text{-amylase}}$ or $EmNMC_{cellulase}$, respectively.

2.5 Nano/microcellulose yield

The yield was determined from small scale experiments, starting with 1 g of five different substrates. These were placed in 50 mL falcons with 20 mL of deionized water, following the same protocol as described in 2.4. Finally, the NMC samples obtained were weighed in order to calculate the extraction yields.

Eqn (1) was applied to calculate the reaction yield from each sample.

$$\text{Nano/microcellulose yield } (\%) = \frac{\text{Nano/microcellulose mass}}{\text{Initial substrate mass}} \times 100 \quad (1)$$

2.6 Fourier-transform infrared spectroscopy

Fourier-transform infrared (FTIR) measurements were performed using a FTIR Spectrometer with an Attenuated Total Reflectance (ATR) accessory (Frontier spectrometer, PerkinElmer). Samples were analyzed by applying a gauge force of 85 at room temperature, acquiring the spectra from 4000 to 650 cm^{-1} at 4 cm^{-1} resolution and 20 scans per sample.

2.7 X-ray diffraction

The X-ray Diffraction (XRD) analyses were carried out using a diffractometer (Empyrean diffractometer, Malvern Panalytical) at 45 kV and 40 mA. The diffraction data of samples were collected at room temperature over a 2θ range of 5–50°. The beam wavelength was 1.5406 Å, the step size was 0.026°, and the time per step was 1.76 s. Then, the crystallinity index (CI_{Segal}) was calculated using the Segal method,[22] as represented in eqn (2).

$$CI_{Segal}\ (\%) = 100 \times \frac{(I_{200} - I_{am})}{I_{200}} \quad (2)$$

where I_{200} is the diffraction signal intensity of the crystalline cellulose, I_{am} is the signal intensity of the amorphous cellulose.

Additionally, a Gaussian deconvolution model was applied to the X-ray spectra. Deconvoluted peaks were used to calculate crystallinity index (CI_{dec}) using eqn (3).[23]

$$CI_{dec}\ (\%) = 100 \times \frac{A_{200}}{A_T} \quad (3)$$

where A_{200} represents the area of the crystalline peak and the A_T is the sum of all the peak areas.

The crystallite size was determined using the Scherrer equation[24] shown in eqn (4).

$$\tau = \frac{k \times \lambda}{\beta \times \cos\theta} \quad (4)$$

where τ is the crystallite size, k, a constant related to the crystallite shape, that is taken as 0.9, according to literature consensus,[25,26] λ is the X-ray wavelength, β is the width of the peak of crystalline cellulose at half of its height and θ is Bragg's angle, the angle between the incident ray and the dispersion planes. The full width at half maximum (FWHM) was determined manually after normalizing the spectra. From the baseline, the height of each crystalline peak was measured and divided by two, and the peak width at this midpoint was then manually measured.

2.8 Thermal analysis

The thermogravimetric analyses (TGA) were performed using a TGA (TGA/DSC 3+, Mettler Toledo). Around 5 mg of each sample were analyzed under a nitrogen atmosphere with a gas flow rate of 50 mL min^{-1}, a heating rate of 10 °C min^{-1}, and a temperature range from 25 to 800 °C.

2.9 Atomic force microscopy

The morphology and size of NMC samples were analyzed by Atomic Force Microscopy (AFM). The concentration of aqueous NMC samples was adjusted to 1% w/v using deionized water. These samples were first sonicated for 30 minutes using 30 second on/off cycles at 30% amplitude. 10 μL of sample were micropipetted and added dropwise onto a mica substrate and dried in a vacuum atmosphere at 30 °C for 24 h. The images were taken using a Multimode AFM system (Multimode 8, Bruker) and Nanoscope V scanning probe microscope (Nanoscope V, Bruker). A TESP-V2 cantilever with a spring constant of 37 N m^{-1} and a frequency of 320 kHz was used to perform these tests. The AFM silicon cantilever has a tip radius of 7 nm and a length of 125 μm. The mean and the standard deviation values of NMC length and diameter were calculated based on measurements from 50 fibers from each sample.

2.10 Scanning electron microscopy

Scanning Electron Microscopy (SEM) in the liquid phase was carried out employing 1% w/v sample solutions using an Environmental Scanning Electron Microscope (ESEM Quanta, Elecmi) equipped with a backscattered electron detector in STEM mode for image acquisition. These samples were sonicated in a sonication bath for 30 minutes with 30 second on/off cycles at 30% amplitude and then they were suspended in water and sandwiched between two amorphous carbon membranes mounted on a 400-mesh copper grid for Transmission Electron Microscopy (TEM) (AGS160-4, Agar Scientific). Measurements were conducted at a chamber pressure of 620 Pa and a 94.5% relative humidity. The system operated at an accelerating voltage of 20 kV and a working distance of 13.3 μm.

2.11 Dynamic light scattering

The size distribution of NMC samples was measured by backscatter Dynamic Light Scattering (DLS) (ZetaSizer Ultra, Malvern Panalytical). Samples were adjusted to a concentration of 0.1% w/v and sonicated in a liquid bath for 30 minutes with 30 second on/off cycles at 30% amplitude. The measurements were

carried out at room temperature, using a beam with a wavelength of 632.8 nm with the beam angle set at 173°.

2.12 Statistical analysis

The results were analyzed using the One-Way Analysis of Variance (ANOVA) statistical model to determine whether the differences between the group means were significant. One-way analysis was performed at a 0.05 level of significance ($p < 0.05$). After the ANOVA analysis, the Tukey test was also performed to identify specifically which group means (among those found to differ significantly by ANOVA) were significantly different from each other. The software used to analyze the dataset was Origin version 8 (OriginLab Corporation, Northampton, USA).

3 Results and discussion

3.1 Nano/microcellulose yield

To verify whether the nanocellulose extraction yields varied significantly depending on the cellulose source, the protocol is described in Section 2.5. for NMC production was conducted. The data obtained are represented in Fig. 2B and C.

No significant differences in yield were observed between the alternative cellulose substrates studied (see above); however, the best yield was obtained at almost all incubation times when filter paper was used as the substrate. As an example, EmNMC after 24 h of incubation increased the reaction yield from around 7.9 ± 2.6%, when no endoglucanase was used, to about 12.4 ± 0.7%, when endoglucanase was used, this being the highest yield of all the series in this work. This result is in agreement with those obtained by Alonso-Lerma *et al.*[20] After analyzing the data statistically, it was determined that the yield difference obtained from EmNMC and when filter paper was used as the substrate was significant (ANOVA, $p < 0.05$). Similar patterns were observed in most of the samples, where the maximum yield was reached after 24 h of incubation, after which it began to decrease. However, the reached yields were not as high as those obtained when employing filter paper as the reaction substrate.

With the aim of comparing the activity of endoglucanase with two other commercial hydrolytic enzymes, α-amylase and cellulase, the same assay applying the same experimental conditions was performed at 3 different incubation times: 5, 24 and 72 h. The yield results are shown in Fig. 2D. Similarly to the blank and experiment with the endoglucanase, the maximum reaction yield was achieved after 24 h of incubation, decreasing when the incubation was longer. This fact could be related to the aggregation of NMC after a long period of stirring.[20] This aggregation was also reported by Khan *et al.*,[27] who obtained similar results when performing acid hydrolysis, attributing this fact to the high abundance of hydroxyl groups in the cellulose. Under the above hypothesis, acid hydrolysis facilitated the formation of hydrogen bonds between cellulose molecules. Li *et al.*[28] showed that, in the presence of NaCl in the NMC suspension, the NMC tended to aggregate. This aggregation could be related to the elution buffer, hindering the activity of the hydrolytic enzymes and decreasing the reaction yield.

The highest yield was 12.4 ± 0.7% with the endoglucanase enzyme after 24 h of incubation, followed by 10.4 ± 1.3% obtained with the α-amylase enzyme after 24 h of incubation. These values were found to be statistically different ($p < 0.05$). Moreover, the extraction yield decreased when the incubation time was longer than 24 h, both without enzymes and with any of the enzymes used.

According to some authors, the presence of cellulose could have an inhibitory effect on α-amylase activity, reducing its extraction yield.[29,30] This fact could be in line with these results, in which the extraction yield obtained was slightly lower than that obtained from EmNMC, clearly observed after 24 h of incubation. Regarding cellulase activity, some authors noted that the production of NMC after short incubation periods was higher than that achieved with longer incubation times, and this has been attributed to the final stage of degradation resulting in glucose monomers rather than the production of only small particles of NMC.[31,32]

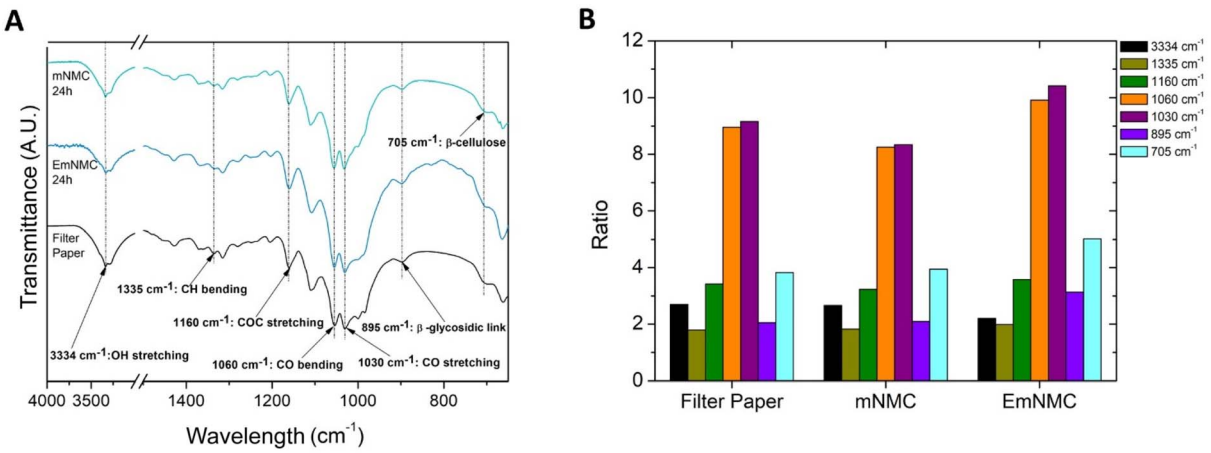

Fig. 3 (A) FTIR spectra of mNMC and EmNMC after 24 h of incubation and filter paper; (B) variations of the indicated mNMC and EmNMC bands intensities, normalized with respect to that of 2903 cm^{-1}, after 24 h of incubation with filter paper as substrate.

Considering that the extraction yield was slightly better when using endoglucanase to degrade filter paper and obtain NMC, the following characterization was carried out with this substrate.

3.2 Fourier-transform infrared spectroscopy

The following graph (Fig. 3A) represents the spectra obtained from FTIR spectroscopy analysis of mNMC, EmNMC, and filter paper. Similar bands appeared in both the substrate and the products, both obtained with enzymes and without them (Fig. S1, S3 and S5†). The study of the differences between the intensity of the stretching and bending bands of each material was performed to understand the structural and molecular composition of the substrates and the samples obtained at different times, both by mechanical forces and by combining mechanical forces and endoglucanase (Fig. S2, S4 and S6†). This analysis also aimed to identify the characteristic functional groups and observe if there were any variations among them, as shown in Fig. 3B, where the characteristic bands of filter paper and mNMC and EmNMC after an incubation of 24 h were compared.

The initial band at 3334 cm^{-1} corresponded to hydroxyl group stretching.[33] The subsequent band at 2903 cm^{-1} corresponded to the stretching of methyl groups.[7] Regarding the fingerprint region, which spanned from 1800 to 600 cm^{-1} and was inherent to each material, several bands stand out. The band at 1635 cm^{-1} was attributed to the bending of hydroxyl groups in water molecules remaining in the material.[2] The bands at 1430 and 1365 cm^{-1} corresponded to CH vibrations,[34] and the one at 1335 cm^{-1} corresponded to the bending of the methyl group.[35] Bands within the range of 1205 to 1000 cm^{-1} aligned with the stretching vibrational bands associated with C–O–C and C–O bonds.[36] Within this range, the band at 1060 cm^{-1} was significant due to the pyranose ring, which was characteristic of the carbohydrates found in the cellulose structure.[37] At 895 cm^{-1}, a subtle band was observed, resulting from the vibration of the β-glycosidic linkage among the monomers constituting cellulose.[12] And, finally, at 705 cm^{-1} the absorption band of β-type cellulose was observed.

The bands shown within the range of 4000–2995 cm^{-1} and at 2903, 1365, 895 and 705 cm^{-1} are essential to determine whether cellulose is in a crystalline or amorphous state.[38] In order to more deeply review whether the enzymatic method for obtaining NMC altered its chemical structure, the ratio between the bands of the functional groups was determined using the methyl group stretching band at 2903 cm^{-1} as a reference. The most relevant ratio differences were shown at 1060, 1030, 895 and 705 cm^{-1}. The band located at 1030 cm^{-1}, characteristic of cellulose type I,[35] indicates the presence of cellulose type I in the samples studied. Zuluaga *et al.*[39] reported that the bands at 750 and 705 cm^{-1} provide information about the conformation of the anomeric carbon, confirming the presence of a phase rich in cellulose I type β, as there is a lack of the band at 750 cm^{-1} representing the α conformation. Lu *et al.*[40] determined that the bands at 1160 and 1060 cm^{-1} correspond to the vibrations of the C–O–C bond between glucose units and the pyranose ring, respectively, and assumed that an increase in the intensity of these bands is associated with a higher content of crystalline cellulose in the sample. Similarly, the same trend is observed in the present work when comparing EmNMC with mNMC, as the intensities of these bands are higher in the sample treated with endoglucanase. However, when compared to the substrate, the intensities remained similar, suggesting that the effect of the enzyme slightly increases the crystallinity relative to mNMC, but not compared to the substrate, as shown in Fig. 3B.

When comparing these results with the band ratios obtained at different incubation times (Fig. S4 and S6†), differences in the band at 895 cm^{-1} could be observed between the mNMC and the EmNMC spectra, with the ratio being slightly higher in the samples treated with endoglucanase. This difference could also be attributed to the extraction process of NMC itself rather than the use of endoglucanase.

To summarize, this was the regular spectrum of cellulose type I, reported by many of the previously mentioned authors. It could also be appreciated that the presence of endoglucanase during the process of obtaining NMC had not resulted in a shift of the functional groups; therefore, its chemical structure was not modified and its β conformation was retained, even when the incubation time increased. Indeed, the spectra of NMCs were quite similar when compared with each other, as well as when compared with the spectrum derived from the substrate.

3.3 Thermogravimetric analysis

TGA was performed to evaluate the effect of the enzyme on the substrates and to prove the thermal stability of the samples. The TGA results of mNMC and EmNMC are represented in Fig. 4A and B. The cellulosic material degradation mechanism has only two stages: (I) light volatiles and residual humidity evaporation; (II) active pyrolysis, corresponding to the decomposition of the cellulose, as the filter paper used as substrate was solely composed of cellulose.[41]

At the beginning of the assay, all the samples exhibited a weight loss at around 63 °C due to the evaporation of residual moisture remaining after lyophilizing the samples. Then, the initial degradation temperature of the samples was around 250 °C and the degradation reaction ended at 375 °C, corresponding to the active pyrolysis stage. This fact is consistent with the results obtained by Chen *et al.*,[42] where it was concluded that the cellulose degradation temperature was from 276 to 407 °C. This behavior was also observed in the samples incubated at different times (Fig. S7–S10†), suggesting that longer incubation times do not affect the thermal stability of the material, as observed in Hernández-Becerra *et al.*[43]

As could be observed, the curves representing the degradation of mNMC exhibited an initial degradation temperature barely higher than that of EmNMC, thus indicating slightly higher thermal stability. Jin *et al.*[44] observed that, when performing enzymatic degradation, cellulose chains could be broken, fracturing parts of the cellulose structure and decreasing the thermal stability of the sample. Considering this, it would be reasonable to expect that with the enzymatic

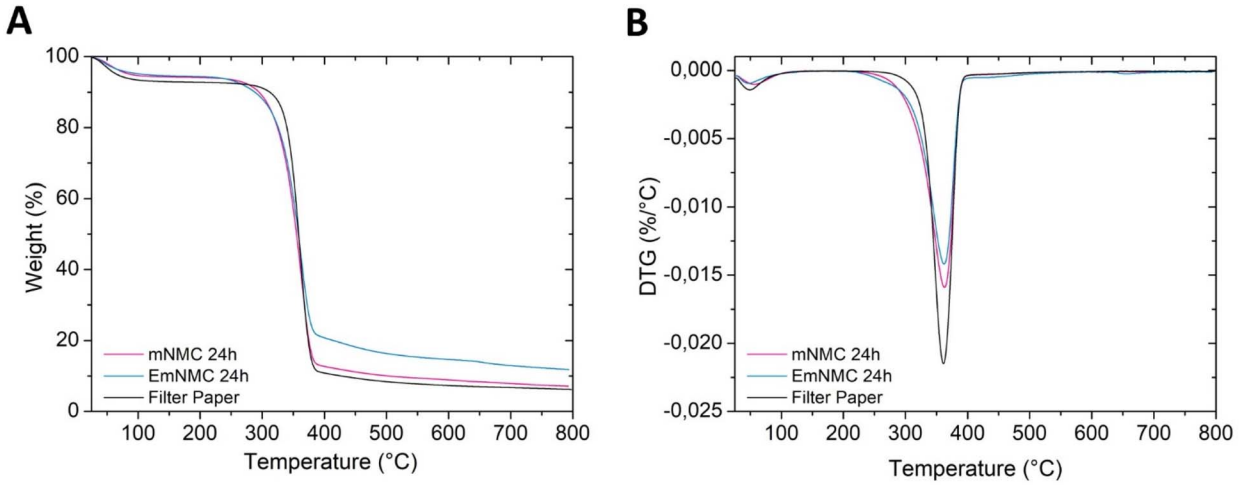

Fig. 4 (A) Weight loss curves and (B) first derivative of the weight loss curves of mNMC, EmNMC, and filter paper.

treatment, the sample degrades at lower temperatures due to its increased accessibility.

At the point where the samples lost 40% of their mass, the curves inverted, with the slope of mNMC increasing, leaving an approximate residue of 9% at 600 °C. However, EmNMC showed a slower mass loss, resulting in a residue of ~15% at the same temperature. This large residue could be due to the presence of enzyme residues (Fig. S11 and S12†). However, for it to be so significant in the case of the NMC, it is possible that the reason for this residue lies elsewhere. It should be noted that similar results were found by other authors.[20]

3.4 Size distribution

The images obtained through AFM and SEM are presented in Fig. 5, showing (A and C) mNMC and (B and D) EmNMC after a 24 h incubation period. As for the NMC length, it could be said that the length of NMC in both samples was in the order

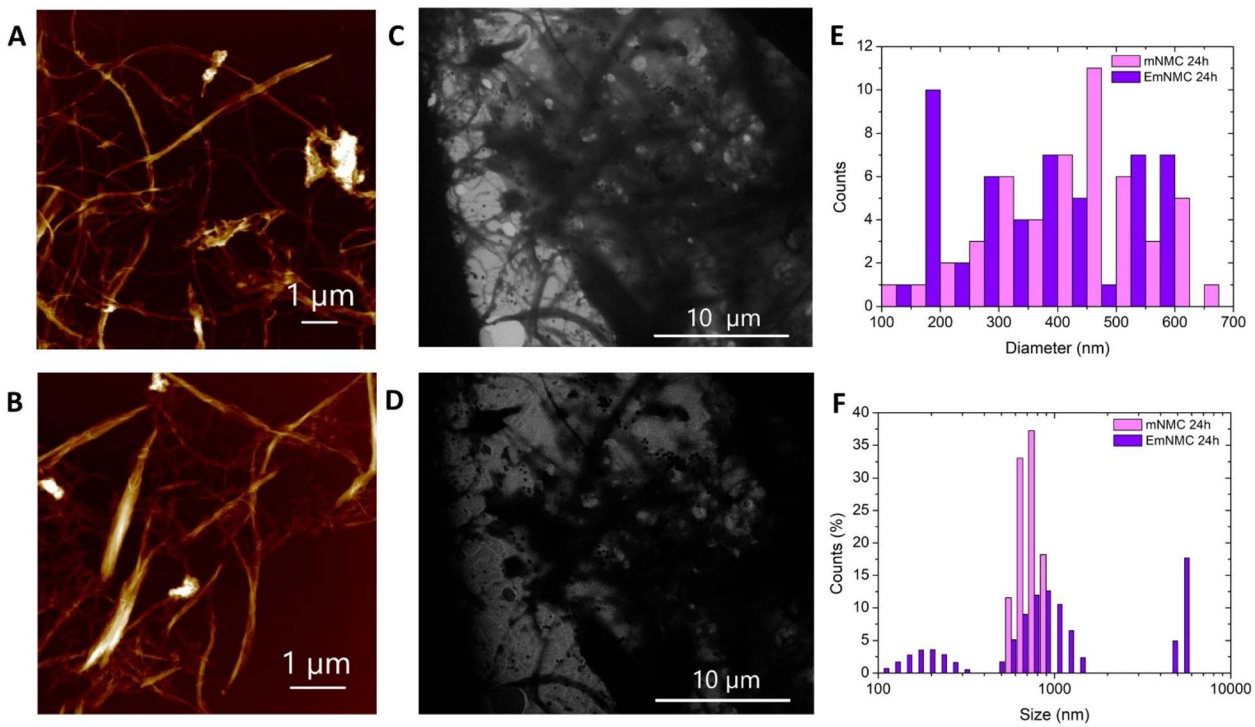

Fig. 5 (A) AFM image of mNMC and (B) EmNMC obtained from filter paper after a 24 h incubation period; SEM images of (C) mNMC and (D) EmNMC obtained from filter paper after a 24 h incubation period; (E) histogram presenting the diameter size distribution of mNMC and EmNMC measured by AFM; (F) size distribution of mNMC and EmNMC measured by DLS.

of microns. However, the diameter of the mNMC fibers was around 441 ± 126 nm, while the diameter of the EmNMC fibers was approximately 360 ± 146 nm. In order to better appreciate the size distribution of both samples, a histogram representing 50 diameter AFM measurements was performed (Fig. 5E). As could be seen, most of the NMC diameters obtained by both methods were between 300 and 600 nm. Concerning EmNMC, the size distribution appeared to consist of slightly smaller sizes (between 300 and 400 nm), while the size distribution of mNMC was between 300 and 600 nm. These values are consistent with the AFM ones obtained by Hernández-Becerra *et al.*[43] The mNMC and EmNMC samples were also analyzed at different extraction times, showing a similar morphology to that of the 24 h samples (Fig. S13 and S14†).

Although it is well known that DLS is suitable for spherical nano-entities, it has also been used for evaluating the size of heterogeneous and larger nanoparticles.[45] A bimodal distribution pattern of EmNMC was confirmed by DLS measurements presented in Fig. 5F. This also occurred in most of the samples incubated at different times that were analyzed (Fig. S15 and S16†). There is no clear pattern in the particle size of the samples, but the average of the smaller particles was around 300 nm and the average of the biggest ones was approximately 800 nm. Reported studies showed that longer mechanical processes do not significantly decrease the particle size.[43] In the case of mNMC, it is very likely that there were also measurements above 1000 nm, but these were probably discarded by DLS software because the correlation model was not the most accurate for samples of this shape. The distribution of small sizes from DLS, measurements between 100 and 1000 nm, approximately corresponded to the diameter distribution measured by AFM. The measurements above that number could be due to the contribution of the length of the NMCs in the samples that were not possible to measure by AFM. These results could indicate that the use of endoglucanase in the extraction process promoted the formation of slightly smaller NMCs compared to those obtained by solely mechanical means.

3.5 X-ray diffraction

To determine the impact of the extraction processes on the crystallinity of the products, the diffraction patterns obtained by XRD of the filter paper were compared with those of mNMC and EmNMC, as illustrated in Fig. 6A. For the diffraction profile of cellulose type I, there were several peaks that must be considered to determine the cellulose pattern in the sample. Those peaks appeared at 14.8° ($1\bar{1}0$), 16.5° (110), 20.6° (102/012), 22.7° (200), and 34.6° (004), where the (200) peak represents crystalline cellulose and the amorphous scattering could be represented by the intensity at the minimum, at about 18.6°, between the (110) and (200) peaks.[46–48]

Regarding the NMC samples produced, both follow the diffraction pattern of the filter paper substrate from which they were produced (Fig. S17†). In addition, the same pattern was also obtained when analyzing mNMC and EmNMC produced using different incubation times (Fig. S18 and S19†). Peak deconvolution was applied in order to isolate and characterize separately the peaks shown in the diffractograms. Initially, the crystallinity index was calculated using the Segal method, which is based on peak intensity values. Then, the X-ray diffraction spectra were deconvoluted, and the crystallinity index was recalculated using the integrated areas of the deconvoluted peaks. In addition, the crystallite size was determined using the Scherrer equation, applying the FWHM of the deconvoluted peaks. The values obtained for mNMC and EmNMC at 24 h incubation time are summarized in Table 1. When comparing the results obtained from both mathematical methods, a similar trend is observed. However, the crystallinity index values calculated through peak deconvolution are significantly lower than those obtained using the Segal method. Park *et al.*[26] investigated this discrepancy and found that, when analyzing the same X-ray diffraction data, the Segal method consistently overestimated crystallinity compared to peak deconvolution analysis. Also, to analyze the behavior of the samples incubated for different periods, the same analysis procedure was applied to all X-ray spectra. The resulting values, used to calculate the crystallinity index, are presented in Table S2.† Huang *et al.*[49] observed a decrease in the crystallinity

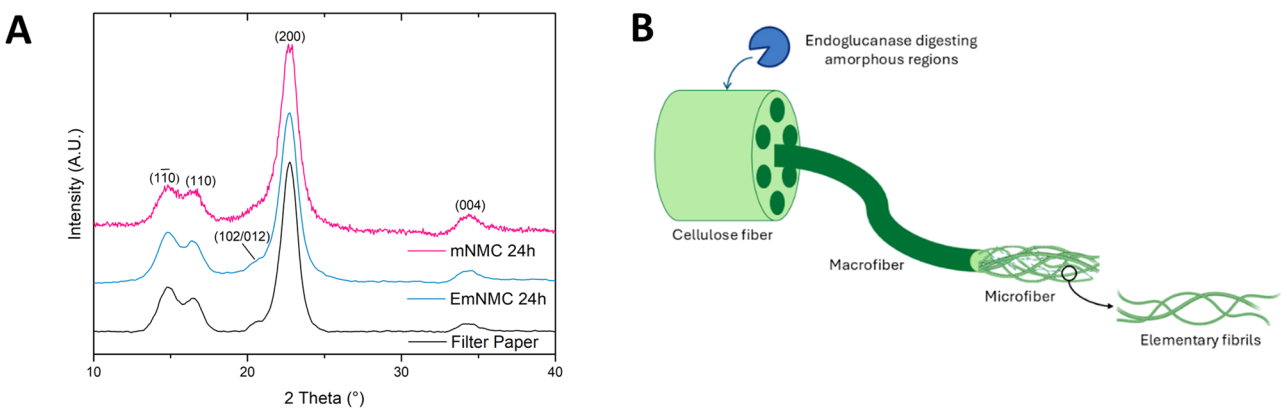

Fig. 6 (A) X-ray diffractograms of mNMC, EmNMC, and filter paper; (B) proposed hypothesis for the nano/microcellulose extraction process, where the dark green areas represent the crystalline regions of cellulose, and the light green areas correspond to the amorphous regions selectively degraded by endoglucanase.

Table 1 Values of crystallinity index obtained by Segal method and by peaks deconvolution, and crystallite size of the mNMC and EmNMC, and filter paper

Sample	Crystallinity index (%) determined by the Segal method	Crystallinity index (%) determined by deconvolution	Crystallite size (nm) determined by deconvolution
mNMC	84	65	7
EmNMC	89	69	7
Filter paper	90	70	6

index over time that was attributed to the partial destruction of the crystalline structure and the production of more disordered regions. This could be the reason why some samples incubated for longer periods have lower crystallinity than others, as shown in Table S2.† Moreover, the crystallinity index of EmNMC was slightly higher than that of mNMC. This fact could point out that the endoglucanase directly targets the amorphous part and the disordered regions of cellulose, because they are more accessible, leaving the crystalline part intact and, thereby, increasing the crystallinity of the sample.[5,31,32] This hypothesis was backed up by the results obtained from FTIR, where slightly higher ratios at 1160 and 1060 cm^{-1} bands were observed in the EmNMC sample, indicating a slightly higher amount of crystalline cellulose in the sample.[40] The hypothesis of nano/microcellulose extraction using endoglucanase is shown in Fig. 6B.

According to results from other authors, the crystallinity index and crystallite size varied significantly depending on the process used to obtain the samples, the pretreatment applied (if any), and other factors, as reviewed by Li *et al.*,[28] who described the treatment, morphology, and crystallite size of the samples. Wang *et al.*[5] hydrolyzed cellulose using both a chemical and a biological process in parallel. The cellulose obtained by both methods was then treated with cellulase and pectinase to produce nanocellulose. After analyzing the two nanocelluloses, they found that the one produced through the chemical method was mainly cellulose type II, while the nanocellulose from the enzymatic method was cellulose type I, which exhibits higher crystallinity than type II. They concluded that the enzyme initially targeted the amorphous part of the cellulose during nanocellulose production, leaving a large part of the crystalline cellulose unhydrolyzed, resulting in higher crystallinity and smaller crystallite size.

Comparing these results to those obtained after analyzing the diffraction patterns, it could be observed that the presence of endoglucanase did affect the crystallinity index of the sample, barely increasing it. In terms of crystallite size, there was no clear trend observed considering that the difference shown between the three samples cannot be considered as representative. Overall, the presence of endoglucanase did not alter the native structure of NMC because the same diffraction pattern was observed. However, slight changes in the crystallinity index suggest that some microstructural modifications might have occurred.

4 Conclusions

This work shows the yield differences of NMC obtained using different hydrolytic enzymes: commercial cellulase and α-amylase and reconstructed endoglucanase. The enzymatic treatment of the cellulosic material (Whatman filter paper) resulted in a slight increase of the extraction yield from approximately 8% without the enzyme, mNMC, to 12% when the endoglucanase enzyme (EmNMC) was used, demonstrating its effect compared to the blank and the commercial hydrolytic enzymes. Additionally, the physicochemical, thermal, and morphological characterization of mNMC and EmNMC revealed a decrease in the average diameter of NMC and an increase in crystallinity for EmNMC compared to mNMC, though not in comparison to the untreated substrate.

In the near future, it would be necessary to consider exploring synergies with other enzymes to further enhance yield in cellulose extraction reactions and try to improve some substrate properties, such as enzyme accessibility or surface functionality, in order to reach significant differences when performing enzymatic extraction. After conducting this study, it would be very necessary to balance the benefits of the use of the enzyme on the efficiency of the extraction process against the costs associated with its use, such as production, purification, *etc.*, due to the modest impact it has had on the extraction process and the material properties.

Data availability

The data supporting this article have been included as part of the ESI.†

Author contributions

Ane Rivas-Zúñiga: methodology, investigation, writing, visualization, formal analysis and funding acquisition. Borja Fernández-d'Arlas: conceptualization, methodology, investigation, supervision, writing, visualization, and formal analysis. Arantxa Eceiza: conceptualization, methodology, investigation, supervision, writing, visualization, formal analysis, and funding acquisition.

Conflicts of interest

The authors declare that they have no financial or personal conflicts of interest that could influence the conduct of this research.

Acknowledgements

This research was financially supported by the Basque Government through the BIKAINTEK program (014-B2/2021) to A. Rivas-Zúñiga. We thank Macrobehavior-Mesostructure-Nanotechnology SGIker unit (UPV/EHU) for technical support

and measurements and N. Barruetabeña for facilitating the endoglucanase phylogenetic tree for its adaptation. A. Eceiza also thanks the Basque Government in the frame of Grupos Consolidados (IT1690-22). The authors thank R. Pérez-Jimenez and the NanoBioTechnology group at CIC nanoGUNE for giving us insights into ancestral enzyme reconstruction, and the Electron Microscopy Laboratory at CIC nanoGUNE for helping out with the SEM measurements. The diagrams shown in this paper were obtained using BioRender software (BioRender, Toronto, Canada).

Notes and references

1 M. Poletto, H. L. Ornaghi Júnior and A. J. Zattera, *Materials*, 2014, **7**, 6105–6119.
2 Y. Cao and H. Tan, *J. Mol. Struct.*, 2004, **705**, 189–193.
3 S. Maiti, J. Jayaramudu, K. Das, S. M. Reddy, R. Sadiku, S. S. Ray and D. Liu, *Carbohydr. Polym.*, 2013, **98**, 562–567.
4 G. Sèbe, F. Ham-Pichavant, E. Ibarboure, A. L. C. Koffi and P. Tingaut, *Biomacromolecules*, 2012, **13**, 570–578.
5 J. Wang, Y. Song, F. Cui, W. Wu, H. Zhu, X. Li and K. Kang, *J. Thermoplast. Compos. Mater.*, 2023, **37**, 1223–1241.
6 B. Aoudi, Y. Boluk and M. Gamal El-Din, *Sci. Total Environ.*, 2022, **843**, 156903.
7 N. Kasyapi, V. Chaudhary and A. K. Bhowmick, *Carbohydr. Polym.*, 2013, **92**, 1116–1123.
8 S. Belbekhouche, J. Bras, G. Siqueira, C. Chappey, L. Lebrun, B. Khelifi, S. Marais and A. Dufresne, *Carbohydr. Polym.*, 2011, **83**, 1740–1748.
9 D. Klemm, F. Kramer, S. Moritz, T. Lindström, M. Ankerfors, D. Gray and A. Dorris, *Angew. Chem., Int. Ed.*, 2011, **50**, 5438–5466.
10 G. Lavrič, A. Oberlintner, I. Filipova, U. Novak, B. Likozar and U. Vrabič-Brodnjak, *Polymers*, 2021, **13**, 2523.
11 W. Wang, M. D. Mozuch, R. C. Sabo, P. Kersten, J. Y. Zhu and Y. Jin, *Cellulose*, 2015, **22**, 351–361.
12 H. S. Onkarappa, G. K. Prakash, G. H. Pujar, C. R. Rajith Kumar, V. Radha, M. S. Latha and V. S. Betageri, *Adv. Nat. Sci. Nanosci. Nanotechnol.*, 2020, **11**, 035001.
13 N. Barruetabeña, B. Alonso-Lerma, A. Galera-Prat, N. Joudeh, L. Barandiaran, L. Aldazabal, M. Arbulu, M. Alcalde, D. De Sancho, J. A. Gavira, M. Carrion-Vazquez and R. Perez-Jimenez, *Commun. Chem.*, 2019, **2**, 76.
14 M. Pääkko, M. Ankerfors, H. Kosonen, A. Nykänen, S. Ahola, M. Österberg, J. Ruokolainen, J. Laine, P. T. Larsson, O. Ikkala and T. Lindström, *Biomacromolecules*, 2007, **8**, 1934–1941.
15 F. Garavand, M. Nooshkam, D. Khodaei, S. Yousefi, I. Cacciotti and M. Ghasemlou, *Adv. Colloid Interface Sci.*, 2023, **318**, 102961.
16 A. Orue, A. Santamaria-Echart, A. Eceiza, C. Peña-Rodriguez and A. Arbelaiz, *J. Appl. Polym. Sci.*, 2017, **134**, 45257.
17 C. D. Midhun Dominic, V. Raj, K. V. Neenu, P. M. S. Begum, K. Formela, M. R. Saeb, D. D. Prabhu, P. Poornima Vijayan, T. G. Ajithkumar and J. Parameswaranpillai, *Int. J. Biol. Macromol.*, 2022, **206**, 92–104.
18 L. Spagnuolo, D. Beneventi, A. Dufresne and A. Operamolla, *ChemistrySelect*, 2024, **9**, e202401511.
19 R. Perez-Jimenez, A. Inglés-Prieto, Z. M. Zhao, I. Sanchez-Romero, J. Alegre-Cebollada, P. Kosuri, S. Garcia-Manyes, T. J. Kappock, M. Tanokura, A. Holmgren, J. M. Sanchez-Ruiz, E. A. Gaucher and J. M. Fernandez, *Nat. Struct. Mol. Biol.*, 2011, **18**, 592–596.
20 B. Alonso-Lerma, L. Barandiaran, L. Ugarte, I. Larraza, A. Reifs, R. Olmos-Juste, N. Barruetabeña, I. Amenabar, R. Hillenbrand, A. Eceiza and R. Perez-Jimenez, *Commun. Mater.*, 2020, **1**, 57.
21 National Center for Biotechnology Information, **https://www.ncbi.nlm.nih.gov/**, accessed 23 October 2024.
22 L. Segal, J. J. Creely, A. E. Martin and C. M. Conrad, *Text. Res. J.*, 1959, **29**, 786–794.
23 P. Scherrer, *Bestimmung der inneren Struktur und der Größe von Kolloidteilchen mittels Röntgenstrahlen*, Springer, Berlin, Heidelberg, 1912.
24 L. Bragg, *The Crystalline State*, George Bell & Sons, London, 1933, vol. 1.
25 A. Monshi, M. R. Foroughi and M. R. Monshi, *World J. Nano Sci. Eng.*, 2012, **2**, 154–160.
26 S. Park, J. O. Baker, M. E. Himmel, P. A. Parilla and D. K. Johnson, *Biotechnol. Biofuels*, 2010, **3**, 10.
27 M. N. Khan, N. Rehman, A. Sharif, E. Ahmed, Z. H. Farooqi and M. I. Din, *Int. J. Biol. Macromol.*, 2020, **153**, 72–78.
28 J. Li, Z. Wang, P. Wang, J. Tian, T. Liu, J. Guo, W. Zhu, M. R. Khan, H. Xiao and J. Song, *Int. J. Biol. Macromol.*, 2024, **258**, 128936.
29 S. Dhital, M. J. Gidley and F. J. Warren, *Carbohydr. Polym.*, 2015, **123**, 305–312.
30 H. Shokrkar and S. Ebrahimi, *Biofuel Bioprod. Biorefining*, 2018, **12**, 749–755.
31 T. Yang, X. Li, N. Xu, Y. Guo, G. Liu and J. Zhao, *Bioresour. Bioprocess*, 2023, **10**, 42.
32 G. A. Siqueira, I. K. R. Dias and V. Arantes, *Int. J. Biol. Macromol.*, 2019, **133**, 1249–1259.
33 R. M. El Sheltami, I. Abdullah and I. Ahmad, *Adv. Mater. Res.*, 2012, **545**, 119–123.
34 P. Satyamurthy, P. Jain, R. H. Balasubramanya and N. Vigneshwaran, *Carbohydr. Polym.*, 2011, **83**, 122–129.
35 C. M. Popescu, M. C. Popescu, G. Singurel, C. Vasile, D. S. Argyropoulos and S. Willfor, *Appl. Spectrosc.*, 2007, **61**, 1168–1177.
36 M. Li, B. He, Y. Chen and L. Zhao, *ACS Omega*, 2021, **6**, 25162–25169.
37 A. Mandal and D. Chakrabarty, *Carbohydr. Polym.*, 2011, **86**, 1291–1299.
38 S. Y. Oh, D. Il Yoo, Y. Shin and G. Seo, *Carbohydr. Res.*, 2005, **340**, 417–428.
39 R. Zuluaga, J. L. Putaux, J. Cruz, J. Vélez, I. Mondragon and P. Gañán, *Carbohydr. Polym.*, 2009, **76**, 51–59.
40 Q. Lu, Z. Cai, F. Lin, L. Tang, S. Wang and B. Huang, *ACS Sustain. Chem. Eng.*, 2016, **4**, 2165–2172.
41 Y. Wang, S. Yang, G. Bao and H. Wang, *J. Anal. Appl. Pyrolysis*, 2024, **178**, 106403.

42 Z. Chen, M. Hu, X. Zhu, D. Guo, S. Liu, Z. Hu, B. Xiao, J. Wang and M. Laghari, *Bioresour. Technol.*, 2015, **192**, 441–450.
43 E. Hernández-Becerra, M. Osorio, D. Marín, P. Gañán, M. Pereira, D. Builes and C. Castro, *Cellulose*, 2023, **30**, 4905–4923.
44 H. Jin, Y. Tian, L. Teng, J. Yang, H. Wu and X. Liu, *Clean Technol. Environ. Policy*, 2025, **27**, 3119–3127.
45 M. J. Huber, N. P. Ivleva, A. M. Booth, I. Beer, I. Bianchi, R. Drexel, O. Geiss, D. Mehn, F. Meier, A. Molska, J. Parot, L. Sørensen, G. Vella, A. Prina-Mello, R. Vogel and F. Caputo, *Anal. Bioanal. Chem.*, 2023, **415**, 3007–3031.
46 Y. Liu and H. Hu, *Fibers Polym.*, 2008, **9**, 735–739.
47 K. S. Salem, N. K. Kasera, M. A. Rahman, H. Jameel, Y. Habibi, S. J. Eichhorn, A. D. French, L. Pal and L. A. Lucia, *Chem. Soc. Rev.*, 2023, **52**, 6417–6446.
48 A. D. French, *Cellulose*, 2014, **21**, 885–896.
49 P. Huang, M. Wu, S. Kuga and Y. Huang, *Cellulose*, 2013, **20**, 2175–2178.